



## RESEARCH LETTER

10.1029/2024GL110285

## How Does Tropical Cyclone-Induced Remote Moisture Transport Affect Precipitation Over East Asia

Shiqi Xiao<sup>1</sup> , Aoqi Zhang<sup>1</sup> , Yilun Chen<sup>1</sup> , Shumin Chen<sup>2</sup>, and Weibiao Li<sup>1,2</sup> <sup>1</sup>School of Atmospheric Sciences, Key Laboratory of Tropical Atmosphere-Ocean System, Ministry of Education, Sun Yat-sen University, Zhuhai, China, <sup>2</sup>Southern Marine Science and Engineering Guangdong Laboratory (Zhuhai), Zhuhai, China

## Key Points:

- TC-induced remote moisture transport frequently occurs over the Yangtze Plain and eastern ocean
- TC-induced remote moisture transport has five main kinds of tracks with different triggering mechanisms
- The orientations further affect precipitation through orographic effects and synoptic circulations

## Supporting Information:

Supporting Information may be found in the online version of this article.

## Correspondence to:

A. Zhang,  
zhangaoq3@mail.sysu.edu.cn

## Citation:

Xiao, S., Zhang, A., Chen, Y., Chen, S., & Li, W. (2024). How does tropical cyclone-induced remote moisture transport affect precipitation over East Asia. *Geophysical Research Letters*, 51, e2024GL110285. <https://doi.org/10.1029/2024GL110285>Received 17 MAY 2024  
Accepted 5 OCT 2024

**Abstract** Analyzing tropical cyclone-induced remote moisture transport clusters (TRCs) and their effects on precipitation is crucial for understanding precipitation formation and enhancing forecast precision. Prior research, primarily case-based, did not fully grasp the nature of TRCs. Utilizing an objective TRC identification method, we categorized 65 TRC tracks in East Asia into five types and examined their traits and precipitation links. The findings indicate that the moisture transport height of TRCs varies due to multiple factors, with higher transport linked to the warm conveyor belt and lower transport attributed to Taiwan's mountain range influencing low-level moisture. The precipitation peak altitudes of TRCs at higher latitudes are greater, and their precipitation intensity is positively correlated with terrain type, especially coastlines. This study underscores the diversity in TRC characteristics and related precipitation, suggesting that future research should consider the directionality of TRC tracks.

**Plain Language Summary** Examining how water vapor is moved far away by large storms called tropical cyclones (TCs) helps us understand how rain is made and helps us better predict it. Earlier studies did not fully understand what these water vapor clusters, or TRCs, were. Therefore, we used a special method to find and sort TRCs. We identified 65 different paths of TRCs in East Asia and divided them into five different groups. We looked at what makes them different and how they are connected to rain. We discovered that the way that high TRCs move water vapor can change because of many factors. Sometimes, a weather pattern called the warm conveyor belt makes the vapor ascend higher. Other times, the mountains in Taiwan affect the lower part of the vapor. Additionally, TRCs in places that are farther from the equator cause increased amounts of rain, and the amount of rain is closely related to the type of terrain, and this phenomenon is especially prominent near coasts. This study shows that there are many different kinds of TRCs and ways that they affect rain. Future research should also look at the paths that TRCs take.

## 1. Introduction

Moisture transport has a significant impact on the global circulation of energy, mass and moisture (Nayak & Villarini, 2017). In recent decades, intense moisture transport has attracted increasing attention, as studies have shown strong association with extreme precipitation and floods at midlatitudes (Gimeno et al., 2016; M. Lu & Hao, 2017). To investigate the statistical characteristics of intense moisture transport (Liang et al., 2022; Wang et al., 2023), identification algorithms have been developed (Collow et al., 2022; Rutz et al., 2019), and their impacts on the atmospheric water cycle and precipitation extremes have been assessed (Gimeno-Sotelo & Gimeno, 2023). Intense moisture transport is generally characterized by transient elongated pathways, concentrated in the lower troposphere (Gimeno et al., 2021).

Tropical cyclones (TCs), the third most common intense global moisture transporters (B. Liu et al., 2020), bring heavy precipitation to coastal and inland areas (M. Lu & Lall, 2017). Additionally, northward ageostrophic winds from TCs can cause torrential rainfall events termed "predecessor rain events" (Bosart et al., 2010; Moore et al., 2013; Saito, 2019; Schumacher et al., 2011). This term refers to precipitation events that separate from TC rainbands and caused by moisture transport originating from a TC, occurring over 700 km away from the center of the TC (L. Chen, 2006; L. Chen et al., 2010; Sun et al., 2017; Xu et al., 2023; L. Yin et al., 2022). Leveraging this insight, we developed the first objective method to identify and quantify the scale, altitude, intensity, and temporal evolution of these TC-induced remote moisture transport (Xiao et al., 2024).

The divergence of upper air moisture from TCs, driven by northward ageostrophic winds and topography, triggers remote heavy rainfall (L. Chen et al., 2010; Chunhua et al., 2011; Saito & Matsunobu, 2020). Research indicates

© 2024. The Author(s).

This is an open access article under the terms of the [Creative Commons Attribution License](#), which permits use, distribution and reproduction in any medium, provided the original work is properly cited.

that such rainfall in South Korea (Baek et al., 2013; Byun & Lee, 2012), Japan (Hirano et al., 2023; Kodama & Satoh, 2022; Saito et al., 2022) and the United States (Bosart et al., 2010, 2012; Schumacher et al., 2011) is mainly due to TC interactions with extratropical systems and intense moisture transport, with minor contribution of topography. In contrast, China's TC-induced remote rainfall events are the results of topographical and synoptic circulation interactions, as exemplified by Typhoon Vicente's (2012) impact on Beijing (Juan et al., 2020; Wen et al., 2015), and Typhoon Mangkhut's (2018) effects on the Yangtze River Delta (Yu et al., 2020; Zuo et al., 2022). The extreme rainfall in Henan from Typhoon In-fa (2021) is attributed to tropical-extratropical interaction and topography in Henan (Xu et al., 2022; J. Yin et al., 2022). Despite these case studies, there remains a need for more quantitative and systematic approach to understanding TC-induced remote heavy rainfall.

To explore the relationship differences among TC-induced remote precipitation and moisture transport and non-TC moisture transport, we objectively identified tracks of TC-induced remote moisture transport that resemble TC tracks. We quantitatively analyzed the relationships between precipitation and the moisture transport features. The rest of the article comprises three sections. Section 2 covers the data and methodology. Section 3 presents the quantified differences in the precipitation–moisture relationship between TC-induced remote moisture transport and non-TC moisture transport. Section 4 contains the conclusion and discussion to reveal the significance of this study and its implications for future research.

## 2. Data and Methods

### 2.1. Data

ERA5 is a global reanalysis data set developed by the European Center for Midrange Weather Forecast (ECMWF) at  $0.25^\circ \times 0.25^\circ$  spatial and one-hour temporal resolutions (Hersbach et al., 2020). We used three-dimensional wind field, specific humidity and geopotential height variables for July–August–September (JAS), 1981–2023 at multiple pressure levels with 6-hr temporal resolution (1981–2020 for statistical analysis and 2021–2023 for validation), as JAS are the three months with the highest TC frequency over the western North Pacific (Demory et al., 2017; Fumin et al., 2002; Xie et al., 2015). These data sets are used to calculate the climatological mean wind field, geopotential height, and vertically integrated moisture transport (IVT) from 1,000 to 300 hPa via the following equations:

$$IVT_u = \frac{1}{g} \int_{1000\text{hPa}}^{300\text{hPa}} qu \, dp, \quad (1)$$

$$IVT_v = \frac{1}{g} \int_{1000\text{hPa}}^{300\text{hPa}} qv \, dp, \quad (2)$$

$$IVT = \sqrt{IVT_u^2 + IVT_v^2}, \quad (3)$$

where  $IVT_u$  ( $IVT_v$ ) represents the zonal (meridional) components of the IVT vector,  $IVT$  represents the magnitude of the IVT vector,  $g$  is gravitational acceleration  $\text{m s}^{-2}$ ,  $u$  and  $v$  are the zonal and meridional layer-mean wind components in  $\text{m s}^{-1}$ ,  $q$  is the layer-mean specific humidity in  $\text{kg kg}^{-1}$ , and  $dp$  is the pressure difference between two adjacent pressure levels in Pa. Positive values of  $IVT_u$  and  $IVT_v$  indicate eastward (northward) zonal (meridional) components.

The best-track TC data set during 1981–2023 is retrieved from the Shanghai Typhoon Institute of the China Meteorological Administration (CMA). We used 6-hourly TC positions, minimum sea level pressure and maximum wind speed throughout the lifecycle of each TC over the western North Pacific (Feng et al., 2014; X. Lu et al., 2021).

The Integrated MultisatellitE Retrievals for Global Precipitation Measurement (GPM-IMERG), funded by NASA and the Japanese Aerospace Exploration Agency (JAXA), offers global precipitation observational data (Pradhan et al., 2022). This product enhances the scope of the Tropical Rainfall Measuring Mission, extending polar observations. We analyzed the calibrated precipitation rate from the final precipitation L3 V07 product in JAS during 2001–2020 for statistical analysis and 2021–2023 for cases, at  $0.1^\circ \times 0.1^\circ$  spatial and 0.5-hr temporal resolutions.

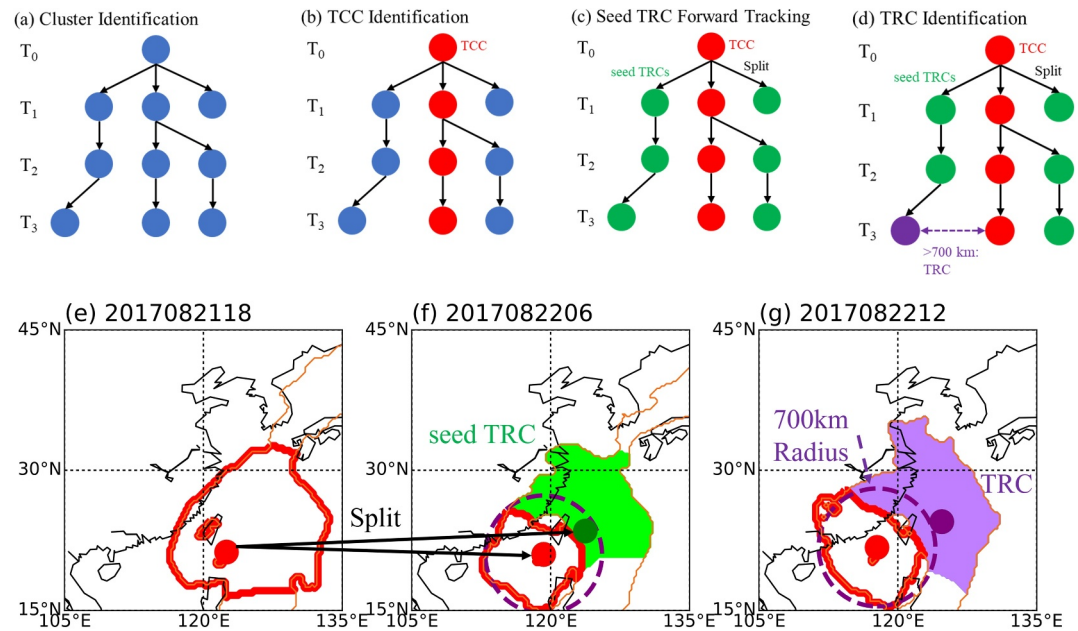


**Figure 1.** Schematic diagram of TRC identification. (a) Identification of clusters (blue), (b) identification of TCCs (red), (c) identification of seed TRCs (green) and forward trackings, (d) identification of TRCs (purple), and (e–g) a real case for the formation of TRC from Typhoon Hato (2017). The black arrows correspond to the temporal split in (c) and (d). The red contours (or clusters), green clusters and purple clusters represent TCCs, seed TRCs and TRCs, respectively. Orange contours represent intense moisture transport. The dashed purple circle represents 700 km radius from the center of TCC.

## 2.2. Methods

TC-induced remote moisture transport occurs outside the TC vicinity, with TC as the moisture source. Following the definition above, we developed the first objective identification method for TC-induced remote moisture transport (Xiao et al., 2024). In this study, we slightly modified this method to identify moisture transport split from TCs as remote transport following the steps:

- (1) Identification of intense moisture transport: regions exceeding the spatiotemporally smoothed 85% quantile IVT values are identified as moisture transport clusters (hereafter clusters), and spatiotemporal digraphs are constructed among the clusters (see Figure 1a).
- (2) Identification of TC clusters (TCCs): the clusters that are nearest to the TC track and less than 150 km away (smaller than typical radius of TCs) are identified as TCCs (see Figure 1b) (Lin et al., 2016; Musgrave et al., 2012).
- (3) Forward tracking of TCCs in the next timestep: we tracked all TCCs ahead of the directed temporal relations by each timestep, and the clusters are identified as seed TC-induced remote moisture transport clusters (seed TRCs) for clusters that are unidentified in Step 2 (see Figure 1c). The first timestep of the TRC track is the TCC where the seed TRC form, and the second timestep is the seed TRC, etc.
- (4) Forward tracking of seed TRCs: for the seed TRCs in Step 3, the branch with the strongest moisture transport is identified. Seed TRCs that are over 700 km from the TCC in the same timestep are identified as TRCs (see Figure 1d). The location of the TRC track is where the IVT is largest over each seed TRC.
- (5) Clusters that are unidentified in Steps 2–4 are non-TCs.

A TCC split into a TCC and TRC(s) when a valley-like (lines of local minima) pattern of IVT values appears in the region of intense moisture transport in the TCC at the next timestep (Figures 1c–1f). The maximum gradient method identifies the sides of the valley as two different clusters (Y. Chen et al., 2020; Xiao et al., 2024). TCC of Hato split into two clusters at 0600 UTC 22 August 2017 (Figure 1f), one TCC (red), and one seed TRC (green), whose distance to TCC exceeded 700 km at 1200 UTC and became the TRC (purple, see Figure 1g).

Using the method above, 329,828 clusters are identified over the western North Pacific and surrounding areas during JAS in 1981–2020, including 325,566 non-TCs, 3,679 TCCs and 583 TRCs. A total of 172,402 clusters are

identified over the same region and during JAS in 2001–2020, including 170,576 non-TCs, 1,573 TCCs and 253 TRCs.

Similar to TC track clustering, we used K-means for TRC track clustering during JAS in 1981–2020 with the following features (Corporal-Lodangco et al., 2014; Y. Yin et al., 2023):

$$\bar{x} = \frac{\sum_{i=1}^l w_i x_i}{\sum_{i=1}^l w(i)}, \quad (4)$$

$$\bar{y} = \frac{\sum_{i=1}^l w_i y_i}{\sum_{i=1}^l w(i)}, \quad (5)$$

$$\text{Var}(x) = \frac{\sum_{i=1}^l w_i (x_i - \bar{x})^2}{\sum_{i=1}^l w(i)}, \quad (6)$$

$$\text{Var}(y) = \frac{\sum_{i=1}^l w_i (y_i - \bar{y})^2}{\sum_{i=1}^l w(i)}, \quad (7)$$

$$\text{Var}(xy) = \frac{\sum_{i=1}^l w_i (x_i - \bar{x})(y_i - \bar{y})}{\sum_{i=1}^l w_i}, \quad (8)$$

where  $l$  is the length of the TRC tracks ( $l \geq 2$ ),  $w_i$  is the square root of the IVT of the cluster,  $x_i$  and  $y_i$  are the longitude and latitude at the  $i$ th timestep of the TRC track. Var represents (co)variance of track location given  $(x_i, y_i)$ . The location and moisture transport intensity of TRCs determine the clustering results.

The mean Silhouette distance method is widely used to determine the optimal number of types in K-means (Y. Yin et al., 2023):

$$S_i = \frac{\min(b_i) - a}{\max[a_i, \min(b_i)]}, \quad (9)$$

$$\bar{S}_k = \frac{1}{n} \sum_{i=1}^n S_i, \quad (10)$$

$$q = \sum_{i=1}^n I(S_i < 0), \quad (11)$$

where  $a_i$  represents the mean distance from the track  $i$  to other tracks within the TRC type,  $b_i$  represents similarly to  $a_i$  but beyond the TRC type. Typically,  $S_i$  range from  $-1$  to  $1$ .  $\bar{S}_k$  is the mean Silhouette value for each  $k$ ,  $q$  represents the number of negative  $S_i$  values,  $I(\text{statement})$  equals to one if the statement is true, otherwise zero.

Specifically, larger  $S_i$  means higher clustering accuracy and larger  $\bar{S}_k$  means more distinguished TRC tracks among different types. We chose  $k$  from 2 to 10 to find the optimal  $k$  value with large  $\bar{S}_k$  and smallest number of negative  $S_i$  values for each  $k$ .

TRC-related precipitation refers to precipitation events occurring TC vicinity and separate from TC rainbands, whose moisture transport sources are TCs. This kind of precipitation is not only triggered by synoptic circulations (Xu et al., 2023; J. Yin et al., 2022), but also affected by orographic effects (C.-S. Chen et al., 2013; Tang & Chan, 2013).

Following the definition above, we associated moisture transport height/intensity, with precipitation over East Asia using GPM-IMERG data during JAS in 2001–2020 as the data is available only from 2001. The median height of IVT, denoted as  $H_{50}$  in km, is determined by its vertical distribution of moisture transport intensity. We used IVT to characterize the intensity. We also took the mean values of precipitation for each cluster and 6-hourly timestep for association with  $H_{50}$  and IVT.

### 3. Results

Figure 2 shows the frequency and resulting precipitation of all clusters and TRCs, and the fraction/contributions of TRCs. The highest all-cluster frequencies are observed in offshore regions in the South China Sea and the East China Sea (Figure 2a, 24%), which echoes previous studies (Gimeno et al., 2016; Park et al., 2021), decreasing toward the open ocean and inland areas. High TRC frequencies (0.5%–1%) are observed over coastal southeastern China, occupying 2%–3% of the all-cluster frequency; large secondary TRC frequencies (0.2%–0.5%) are observed in the regions north of the Nanling Mountains in China, accounting for 1%–2% of the all-cluster frequency (see Figures 2b and 2c). This paper selects the area denoted as the TRC-frequent region (TFR) with high TRC frequencies at 110–130°E, 22–40°N (black dashed line), which mainly includes central and eastern China, and the Korean Peninsula.

Cluster/TRC-related 6-hourly precipitation is the grid-wise precipitation amount in the next 6 hr at the area of each cluster/TRC for analysis of TRC contribution to precipitation to all clusters in JAS during 2001–2020 (see Figures 2d–2f). The overall precipitation increases toward coastal areas and lower latitudes, peaking at 1,000 mm yr<sup>-1</sup> in the northern South China Sea and secondary peak of 400–700 mm yr<sup>-1</sup> over the Korean Peninsula and surroundings (see Figure 2d), consistent with typical late-summer patterns in East Asia (Demory et al., 2017; Park et al., 2021). Similar to Figure 2b, the peak (10–30 mm yr<sup>-1</sup>) of TRC-related precipitation is concentrated in the East China Sea and Korean Peninsula (as shown in Figure 2e), echoing findings in previous studies (Baek et al., 2013; Byun & Lee, 2012; J. Yin et al., 2022; Yu et al., 2020; Zuo et al., 2022). The contribution distribution of TRC-related precipitation mirrors the annual mean (Figure 2e), with 3%–10% at coastal regions in eastern China, South Korea, and western Japan, and lower inland values (0.3%–2%) in central China (see Figure 2f).

Similar to previous definitions (Pan & Lu, 2019; Xiao et al., 2024), precipitation exceeding local 99.5% quantile threshold over 2001–2000 is extreme precipitation. The overall distribution of extreme precipitation (see Figure 2g) is similar to that of all precipitation (see Figure 2d), but with primary peak of 300 mm yr<sup>-1</sup> in western Philippines and secondary peak of 120–240 mm yr<sup>-1</sup> over the Korean Peninsula. The primary large values of TRC-related extreme precipitation are 10–20 mm yr<sup>-1</sup> over East China Sea (see Figure 2h). The contribution distribution of TRC-related extreme precipitation resembles that in Figure 2f, with over 10% offshore, and 1%–5% inland (Figure 2i), roughly three times of TRC contribution to all precipitation (Figure 2f).

We used K-means on TRC tracks passing the TFR in 1981–2020 to further investigate differences in the association between rainfall and moisture transport height/intensity among TRCs and non-TCs (see Figures 3a–3f). Results show that 5 is the optimal  $k$  value with large mean Silhouette value over 0.4 (distinguished TRC types) and only one negative  $S_i$  value (Figure S2 in Supporting Information S1). There are few TRC tracks inland in 2001–2020 (Figure S3 in Supporting Information S1), likely causing small TRC annual mean precipitation inland (Figures 2e and 2h).

The first type NE (14 tracks, 21.53%) characterizes TRCs formed from TCs in coastal South China, moving northeastward within China (see Figure 3a). Specifically, a typical instance of TRC formed from TC Zeke (1991) under the effect of steering flow at northwestern flank of the subtropical high (5,880 m) at 500 hPa, covering southwestern and central China (see Figure S4a in Supporting Information S1). The median  $H_{50}$  and IVT values are 2.49 km and 610 kg m<sup>-1</sup> s<sup>-1</sup>, respectively.

The second type DistNE (3 tracks, 4.6%) characterizes TRCs formed from TCs located similar to NE. However, these tracks can reach Korea and Japan (see Figure 3b). The type of DistNE forms from the prevailing westerly jet

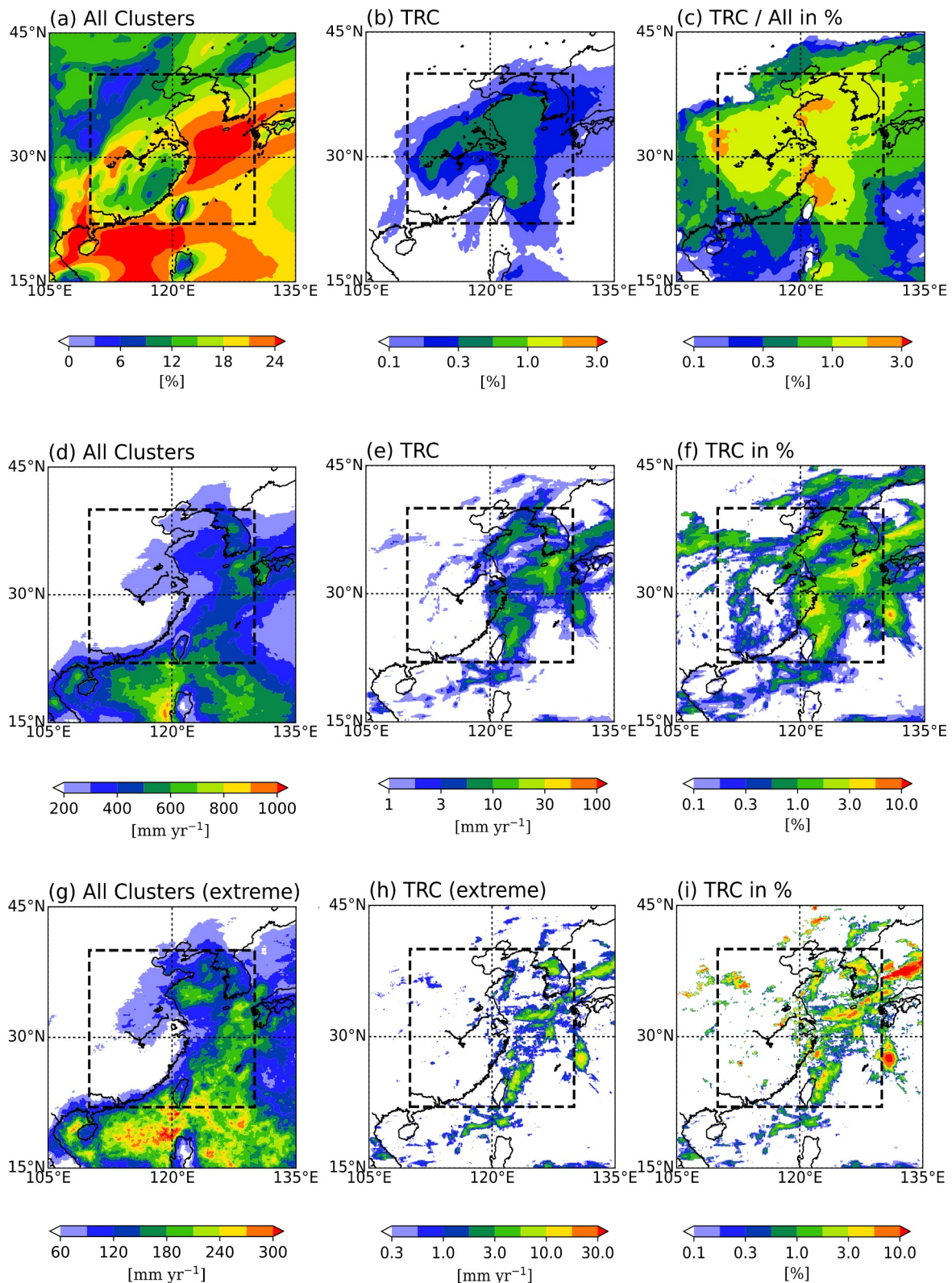


**Figure 2.** Frequency of (a) all clusters; (b) TRCs; (c) fraction of TRCs among clusters. Annual mean precipitation of (d) all clusters; (e) TRCs and (f) contribution of TRCs to precipitation induced by all clusters. The black dashed box indicates the TFR. (g)–(i) are similar to (d)–(f) but for extreme precipitation.

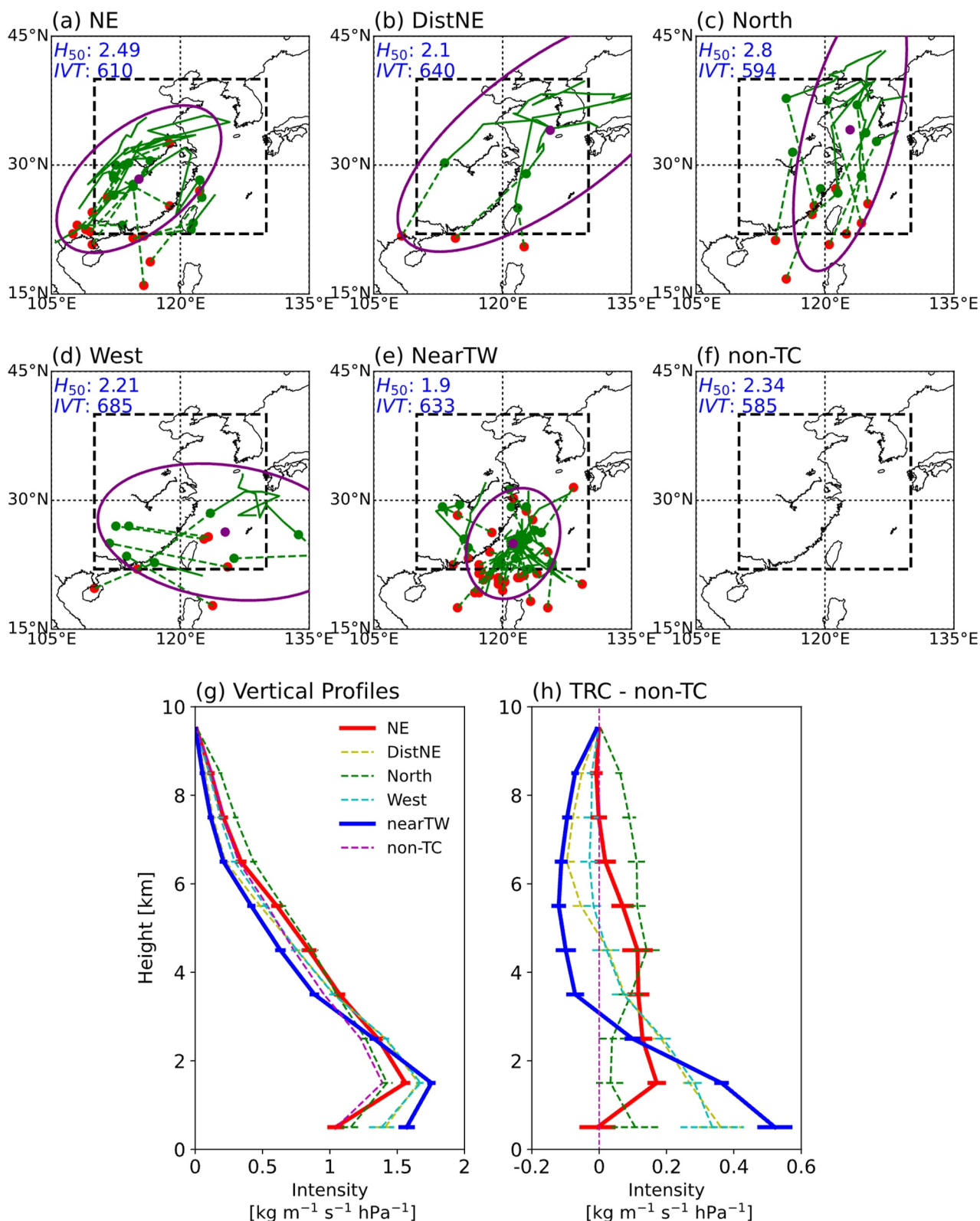


**Figure 3.** The classification results of TRC tracks including: (a) NE, (b) DistNE, (c) North, (d) West, and (e) NearTW, and (f) the horizontal ranges of non-TC samples. Red represents TCCs that TRCs (in green) form from. Green dashed lines connect TCCs and the first timestep of TRCs. Purple shows the oval from covariance matrices, showing the orientations of TRC tracks. (g) Vertical profiles and (h) deviation from non-TC samples.  $H_{50}$  and IVT represent median values of moisture transport height and intensity in each type, respectively. The bars in (g) and (h) show confidence intervals using standard error.

that split part of the moisture from TCs. The TRC formed from the TCC 08w (2000) (see Figure S5 in Supporting Information S1) affected regions from southeastern China to eastern Japan along the jet (see Figure S4b in Supporting Information S1). The median  $H_{50}$  and IVT values are 2.1 km and  $640 \text{ kg m}^{-1} \text{ s}^{-1}$ , respectively.

North (9 tracks, 13.8%) forms from TCCs less than 1,000 km away from Taiwan Island. The North type of TRC tracks move northward along the coastline in China (see Figure 3c), likely due to strong northward moisture transport at the western flank of northernmost subtropical high, splitting part of the moisture of the TC away. The TRC formed from TC Matsa (2005) reached deep inland areas in northeastern China, with 6-hourly mean precipitation of 10–25 mm over the lifetime of TRCs (see Figure S4c in Supporting Information S1). The median  $H_{50}$  and IVT values are 2.8 km and  $560 \text{ kg m}^{-1} \text{ s}^{-1}$ , respectively.

The West (8 tracks, 12.3%) type mostly moves westward with typical lifetimes less than 12 hr, mainly affecting southeastern coastal China (see Figure 3d). The formation of West is likely due to weak steering flow in the southwestern flank of the subtropical high, resulting in unfavorable conditions for formation and a short lifetime of TRCs. However, the TRC formed from TC In-fa (2021) is an exception, beyond 1981–2000. The long lifetime (36 hr) of the TRC is attributed to strong steering flow, bringing 6-hourly mean precipitation of 25–50 mm over Henan Province (see Figure S4d in Supporting Information S1). The median  $H_{50}$  and IVT values are 2.21 km and  $685 \text{ kg m}^{-1} \text{ s}^{-1}$ , respectively.

NearTW (31 tracks, 47.69%) dominates the TRCs, located within a 1,200 km radius centered on Taiwan Island, where these tracks pass (Figure 3e). One typical example of the NearTW type was split from TC Mangkhut (2018), where mountains in Taiwan deflected part of moisture northwards to Yangtze River Delta (see Figure S4e in Supporting Information S1). This TRC brought 6-hourly mean precipitation of 10–25 mm in Yangtze River Delta (Yu et al., 2020; Zuo et al., 2022). The median  $H_{50}$  and IVT values are 1.9 km and  $633 \text{ kg m}^{-1} \text{ s}^{-1}$ , respectively.

The orientations of the TRC tracks determined by K-means highly echo those of the TC tracks using K-means in previous studies, likely because of the similar synoptic background affecting the TRCs to that affecting the TCs (Y. Yin et al., 2023).

The median of  $H_{50}$  values for NE and North is the highest of 2.34 km (see Figure S6a in Supporting Information S1), possibly due to Warm Conveyor Belts (WCB) elevating moisture at higher latitudes (Dacre et al., 2019; Pickl et al., 2023). NearTW exhibits the lowest  $H_{50}$ , likely because Taiwan's mountains diverge TC moisture (C.-S. Chen et al., 2013; Huang & Dong, 2019; Tang & Chan, 2013). The median IVT of five TRC types is slightly higher than non-TCs, with West's highest peak and North's wider range (see Figure S6b in Supporting Information S1), suggesting strong tropical-extratropical air interactions. NearTW's shorter distance to TCCs (median 900 km) compared to other TRC types (median 1,100–2,000 km), implies a larger tangential wind component (Chavas et al., 2017) and stronger topographical moisture divergence, with weaker association with 500 hPa circulation (see Figure S6c in Supporting Information S1).

We further analyzed vertical distribution of moisture transport intensity among TRCs and non-TCs in Figures 3g and 3h. The intensity ranges between 1.4 and  $1.8 \text{ kg m}^{-1} \text{ s}^{-1}$  over the TFR at 1–2 km altitude, decreasing with height (Figure 3g). NE shows larger intensity than non-TCs at all levels, peaking at  $0.2 \text{ kg m}^{-1} \text{ s}^{-1}$  deviation at 1–2 km (Figure 3h). North shows largest intensity deviation from non-TCs at 4–5 km altitudes, possibly due to WCB influence, elevating poleward moisture transport (Dacre et al., 2019; Heitmann et al., 2024). DistNE and West have greater intensity than non-TC up to 5 km, with the largest deviation of  $0.35 \text{ kg m}^{-1} \text{ s}^{-1} \text{ hPa}^{-1}$  at 0–1 km (Figure 3h). In contrast, NearTW has larger intensity below 1 km by over  $0.5 \text{ kg m}^{-1} \text{ s}^{-1} \text{ hPa}^{-1}$  but lower at 3–10 km, especially at 5–6 km, which is attributed to Taiwan's mountain-induced precipitation from TC-transported moisture below 3 km.

We computed 6-hourly cumulative precipitation averaged at the cluster ( $R_6$ ) area, and related it to  $H_{50}$  and IVT (separately) using nonlinear functions, which are widely used in various scientific fields (Anniballe & Bonafoni, 2015; Bartók & Csányi, 2015; Massicotte & Markager, 2016). This approach aims to explore the quantitative link between rainfall and moisture transport features. There is a multimodal relationship between  $R_6$  and  $H_{50}$ , with peak precipitation at varying levels like 900–1,000 and 300–400 hPa in a recent study (T. Liu et al., 2023). Given the scatter plot's distribution, a superposition of Gaussian functions is optimal for their continuous differentiability. For  $R_6$  and IVT values far beyond cluster identification thresholds, we used multiples of the sigmoid function, featuring continuous differentiability, pseudo-exponential growth, and the zero-to-one range.

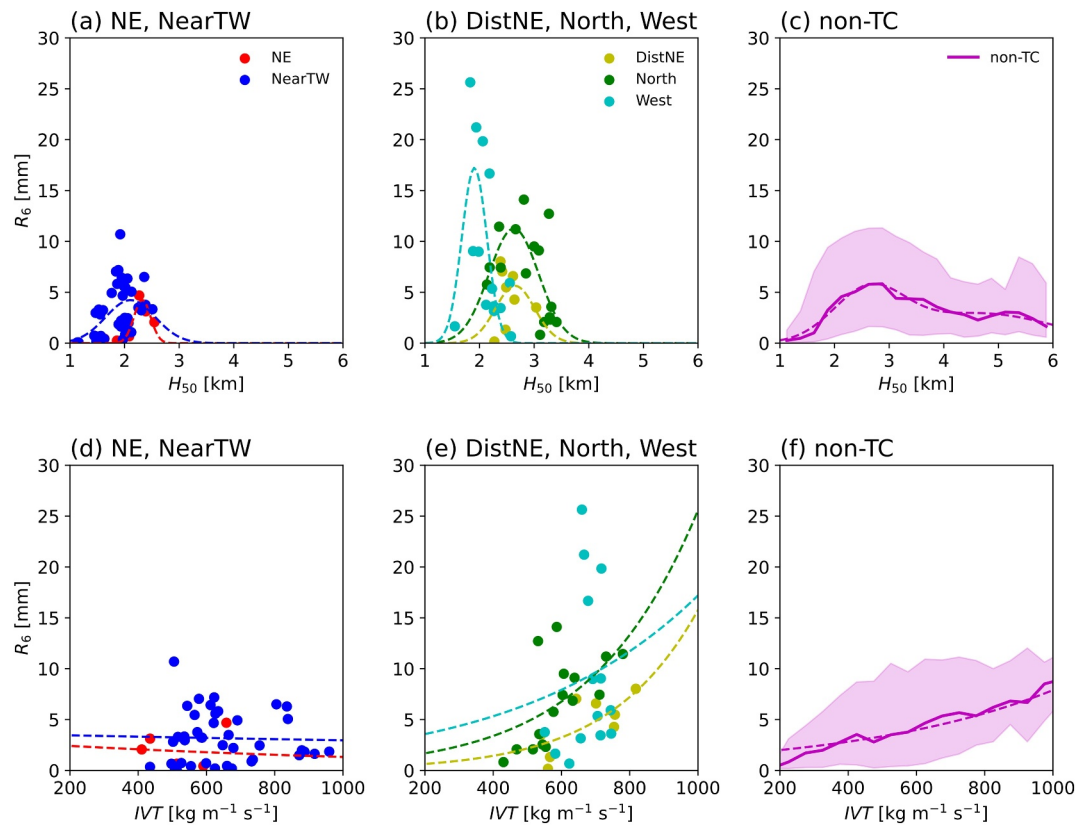


**Figure 4.** Scatter plots of the cluster precipitation amount  $R_6$  with (a–c) median IVT height  $H_{50}$  and with (d–f) intensity IVT and corresponding fit lines (dashed lines). (a, d) The characteristics of NE and NearTW, (b, e) DistNE, North and West, and (c, f) non-TCs. The thick solid line indicates the median values of non-TCs. The shading represents the range of 10%–90% quantiles, and the dashed line represents the fitting curve.

We analyzed the functional relationships between  $R_6$ , and  $H_{50}$  and IVT (separately) for five types of TRCs and non-TCs during JAS in 2001–2020 (see Figure 4). The TRCs show single-peaked Gaussian characteristics, with peaks at 6 mm for NE and 5 mm for NearTW (Figure 4a), implying complex factors for NearTW precipitation. DistNE and North have higher  $R_6$  peaks at about 2.7 km  $H_{50}$  (Figure 4b), possibly influenced by strong extratropical cyclones. North and West have higher  $R_6$  peaks of 17 and 12 mm, respectively (Figure 4b), echoing the precipitation patterns in Figures 2e and 2f. This may be because the North, similar to Typhoon Ampil (2018), continuously receives moisture offshore and is influenced by the WCB (Dacre et al., 2019; Pickl et al., 2023); the West is located on the southwestern flank of the subtropical high, where strong tropical convection fosters heavy rainfall. Non-TC displays a double-peaked Gaussian distribution with  $R_6$  peaks at 12 mm at 2.7 km and 8 mm at 5.5 km (Figure 4c).

Fitting the relation between  $R_6$  and IVT using sigmoid functions, there is insignificant positive correlation (Table S1 in Supporting Information S1) for NE and NearTW (Figure 4d), due to few samples for NE and orographic lifting effect for NearTW, possibly resulting in weak IVT but heavy rainfall. North, DistNE, West, and non-TC show positive correlations from strong to weak (Figures 4e and 4f). This may be because North and DistNE are greatly influenced by the underlying surface, with strongest positive correlation between precipitation with IVT near the coastline (Figures 2e, 2f, 3b, and 3c); the West, located mostly over the ocean, has a large precipitation with small IVT, showing a weaker positive correlation (Figures 2e and 2f).

#### 4. Conclusions

Understanding the characteristics of TC-induced remote moisture transport and its connection to precipitation is crucial. Based on Xiao et al. (2024), this study objectively identified TRC tracks affecting East Asia during JAS in 1981–2020, and 2021–2023 for case validation. Subsequently, using GPM-IMERG precipitation observation data

sets and ERA5, the 6-hr cumulative precipitation, moisture transport height and intensity for all clusters are calculated to obtain the following main conclusions:

- Clusters in the eastern and southern TFRs occur more frequently, with a higher TRC frequency in the east than in the south, resembling the distribution of annual mean rainfall. Although TRCs occupies 3% of strong moisture transport, they contribute 10% to the all-cluster-induced total rainfall, and more for extreme rainfall, indicating above-average intensity of TRC-related precipitation. This result highlights the importance of studying TRC characteristics to understand TRC-related precipitation.
- TRC tracks are classified into five types using K-means: NE, DistNE, North, West, and NearTW, consistent with previous TC track clustering (Y. Yin et al., 2023). NE and North TRCs show higher moisture transport than non-TCs, likely due to WCB's moisture elevation. NearTW has the lowest moisture transport from TC moisture and Taiwan's mountain divergence. Moisture transport of TRCs is stronger than non-TCs. NE and North feature broader distributions and higher limits, while West has a higher median but lower maximum, possibly due to tropical-extratropical interactions.
- Gaussian function is used to examine the link between precipitation amount and the moisture transport height. The North and West experience the most rainfall, owing to a steady marine moisture supply and tropical convection. The DistNE and North show the highest peak precipitation heights, with predominance of extratropical cyclones. Precipitation is also correlated with transport intensity using pseudoexponential function. NE and NearTW show insignificant correlation (Gimeno-Sotelo & Gimeno, 2023; M. Lu & Lall, 2017), likely due to the NE's small sample size and Taiwan's orographic effects. Contrastly, North and DistNE demonstrate a strong positive correlation, potentially linked to terrain variations, particularly near coasts.

The results and conclusions provide a solid theoretical foundation for understanding the underlying mechanisms and for precipitation forecasting. However, the study has the following limitations. Only TCs in the northwestern Pacific are considered in this study. We neglected impacts on East Asia by TCs over the Indian Ocean. Small TRC sample sizes and biased sample proportions of TRCs and non-TCs under various clustering may be future research topics for higher accuracy in TC-induced remote precipitation forecasting.

## Data Availability Statement

We appreciate the ECMWF for providing ERA5 reanalysis data available in Hersbach et al. (2023), NASA and JAXA for providing the GPM-IMERG precipitation observational data available in Huffman et al. (2019), and the CMA for providing TC best-track data (X. Lu et al., 2021).

## References

- Anniballe, R., & Bonafoni, S. (2015). A stable Gaussian fitting procedure for the parameterization of remote sensed thermal images. *Algorithms*, 8(2), 82–91. <https://doi.org/10.3390/a8020082>
- Baek, E.-H., Kim, J.-H., Kug, J.-S., & Lim, G.-H. (2013). Favorable versus unfavorable synoptic backgrounds for indirect precipitation events ahead of tropical cyclones approaching the Korean Peninsula: A comparison of two cases. *Asia-Pacific Journal of Atmospheric Sciences*, 49(3), 333–346. <https://doi.org/10.1007/s13143-013-0032-z>
- Bartók, A. P., & Csányi, G. (2015). Gaussian approximation potentials: A brief tutorial introduction. *International Journal of Quantum Chemistry*, 115(16), 1051–1057. <https://doi.org/10.1002/qua.24927>
- Bosart, L. F., Cordeira, J. M., Galarneau, T. J., Moore, B. J., & Archambault, H. M. (2012). An analysis of multiple predecessor rain events ahead of tropical cyclones Ike and Lowell: 10–15 September 2008. *Monthly Weather Review*, 140(4), 1081–1107. <https://doi.org/10.1175/mwr-d-11-00163.1>
- Bosart, L. F., Galarneau, T. J., & Schumacher, R. S. (2010). Predecessor rain events ahead of tropical cyclones. *Monthly Weather Review*, 138(8), 3272–3297. <https://doi.org/10.1175/2010mwr3243.1>
- Byun, K.-Y., & Lee, T.-Y. (2012). Remote effects of tropical cyclones on heavy rainfall over the Korean peninsula—Statistical and composite analysis. *Tellus A: Dynamic Meteorology and Oceanography*, 64(1), 14983. <https://doi.org/10.3402/tellusa.v64i0.14983>
- Chavas, D. R., Reed, K. A., & Knaff, J. A. (2017). Physical understanding of the tropical cyclone wind-pressure relationship. *Nature Communications*, 8(1), 1360. <https://doi.org/10.1038/s41467-017-01546-9>
- Chen, C.-S., Lin, Y.-L., Zeng, H.-T., Chen, C.-Y., & Liu, C.-L. (2013). Orographic effects on heavy rainfall events over northeastern Taiwan during the northeasterly monsoon season. *Atmospheric Research*, 122, 310–335. <https://doi.org/10.1016/j.atmosres.2012.10.008>
- Chen, L. (2006). The evolution on research and operational forecasting techniques of tropical cyclones. *Journal of Applied Meteorological Science*, 17(6), 672–681.
- Chen, L., Li, Y., & Cheng, Z. (2010). An overview of research and forecasting on rainfall associated with landfalling tropical cyclones. *Advances in Atmospheric Sciences*, 27(5), 967–976. <https://doi.org/10.1007/s00376-010-8171-y>
- Chen, Y., Chen, G., Cui, C., Zhang, A., Wan, R., Zhou, S., et al. (2020). Retrieval of the vertical evolution of the cloud effective radius from the Chinese FY-4 (Feng Yun 4) next-generation geostationary satellites. *Atmospheric Chemistry and Physics*, 20(2), 1131–1145. <https://doi.org/10.5194/acp-20-1131-2020>

## Acknowledgments

This research is funded by the Guangdong Major Project of Basic and Applied Basic Research (Grant 2020B0301030004), the National Natural Science Foundation of China (Grants 42075004 and 42475085), the Innovation Group Project of the Southern Marine Science and Engineering Guangdong Laboratory (Zhuhai) (Grant 311022006), and the Open Project of China Meteorological Administration Basin Heavy Rainfall key Laboratory (2023BHR-Z04). This work is part of Shiqi Xiao's doctoral thesis.

- Chunhua, C., Lianshou, C., Xiaotu, L., & Ying, L. (2011). An overview on study in tropical cyclone remote rainfall. In *Paper presented at the 2nd WMO international workshop on tropical cyclone landfall processes (IWTCLP-II)*.
- Collow, A. B. M., Shields, C. A., Guan, B., Kim, S., Lora, J. M., McClenny, E. E., et al. (2022). An overview of ARTMIP's tier 2 reanalysis intercomparison: Uncertainty in the detection of atmospheric rivers and their associated precipitation. *Journal of Geophysical Research: Atmospheres*, 127(8), e2021JD036155. <https://doi.org/10.1029/2021jd036155>
- Corporal-Lodangco, I. L., Richman, M. B., Leslie, L. M., & Lamb, P. J. (2014). Cluster analysis of North Atlantic tropical cyclones. *Procedia Computer Science*, 36, 293–300. <https://doi.org/10.1016/j.procs.2014.09.096>
- Dacre, H. F., Martínez-Alvarado, O., & Mbengue, C. O. (2019). Linking atmospheric rivers and warm conveyor belt airflows. *Journal of Hydrometeorology*, 20(6), 1183–1196. <https://doi.org/10.1175/jhm-d-18-0175.1>
- Demory, M.-E., Turner, A. G., Vidale, P. L., Klingaman, N. P., Guo, L., & Cobb, A. (2017). Contribution of tropical cyclones to atmospheric moisture transport and rainfall over East Asia. *Journal of Climate*, 30(10), 3853–3865. <https://doi.org/10.1175/jcli-d-16-0308.1>
- Feng, J., Lu, X., Yu, H., Zhang, W., Ying, M., Fan, Y., et al. (2014). An overview of the China meteorological administration tropical cyclone database. *Journal of Atmospheric and Oceanic Technology*, 31(2), 287–301. <https://doi.org/10.1175/jtech-d-12-00119.1>
- Fumin, R., Gleason, B., & Easterling, D. J. A. I. A. S. (2002). Typhoon impacts on China's precipitation during 1957–1996. *Advances in Atmospheric Sciences*, 19(5), 943–952. <https://doi.org/10.1007/s00376-002-0057-1>
- Gimeno, L., Algarra, I., Eiras-Barca, J., Ramos, A. M., & Nieto, R. (2021). Atmospheric river, a term encompassing different meteorological patterns. *WIREs Water*, 8(6). <https://doi.org/10.1002/wat2.1558>
- Gimeno, L., Dominguez, F., Nieto, R., Trigo, R., Drumond, A., Reason, C. J. C., et al. (2016). Major mechanisms of atmospheric moisture transport and their role in extreme precipitation events. *Annual Review of Environment and Resources*, 41(1), 117–141. <https://doi.org/10.1146/annurev-environ-110615-085558>
- Gimeno-Sotelo, L., & Gimeno, L. (2023). Where does the link between atmospheric moisture transport and extreme precipitation matter? *Weather and Climate Extremes*, 39, 100536. <https://doi.org/10.1016/j.wace.2022.100536>
- Heitmann, K., Sprenger, M., Binder, H., Wernli, H., & Joos, H. (2024). Warm conveyor belt characteristics and impacts along the life cycle of extratropical cyclones: Case studies and climatological analysis based on ERA5. *Weather and Climate Dynamics*, 5(2), 537–557. <https://doi.org/10.5194/wcd-5-537-2024>
- Hersbach, H., Bell, B., Berrisford, P., Biavati, G., Horányi, A., Muñoz Sabater, J., et al. (2023). ERA5 hourly data on single 507 levels from 1940 to present. *Copernicus Climate Change Service (C3S) Climate Data Store (CDS)*. <https://doi.org/10.24381/cds.bd0915c6>
- Hersbach, H., Bell, B., Berrisford, P., Hirahara, S., Horányi, A., Muñoz-Sabater, J., et al. (2020). The ERA5 global reanalysis. *Quarterly Journal of the Royal Meteorological Society*, 146(730), 1999–2049. <https://doi.org/10.1002/qj.3803>
- Hirano, S., Ito, K., & Yamada, H. (2023). Tropical cyclone track modified by a front located to the northeast. *Sola*, 19(0), 109–115. <https://doi.org/10.2151/sola.2023-015>
- Huang, W., & Dong, S. (2019). Long-term and inter-annual variations of tropical cyclones affecting Taiwan region. *Regional Studies in Marine Science*, 30, 100721. <https://doi.org/10.1016/j.rsma.2019.100721>
- Huffman, G. J., Stocker, E. F., Bolvin, D. T., Nelkin, E. J., & Tan, J. (2019). GPM IMERG late precipitation L3 half 514 hourly 0.1 degree x 0.1 degree V06, Greenbelt, MD. *Goddard Earth Sciences Data and Information Services Center (GES DISC)*. <https://doi.org/10.5067/GPM/IMERG/3B-HH-L/06>
- Juan, L. I., Xiang-de, X. U., Yue-qing, L. I., Tian-liang, Z., & Chong, W. U. (2020). The key supply source of long-distance moisture transport for the extreme rainfall event on July 21, 2012 in Beijing. *Journal of Tropical Meteorology*, 26(3), 34–47. <https://doi.org/10.46267/j.1006-8775.2021.004>
- Kodama, S., & Satoh, M. (2022). Statistical analysis of remote precipitation in Japan caused by typhoons in September. *Journal of the Meteorological Society of Japan. Ser. II*, 100(6), 893–911. <https://doi.org/10.2151/jmsj.2022-046>
- Liang, J., Yong, Y., & Hawcroft, M. K. (2022). Long-term trends in atmospheric rivers over East Asia. *Climate Dynamics*, 60(3–4), 643–666. <https://doi.org/10.1007/s00382-022-06339-5>
- Lin, N., Chavas, D. R., Dong, W., & Lin, Y. (2016). Observed tropical cyclone size revisited. *Journal of Climate*, 29(8), 2923–2939. <https://doi.org/10.1175/jcli-d-15-0731.1>
- Liu, B., Tan, X., Gan, T. Y., Chen, X., Lin, K., Lu, M., & Liu, Z. (2020). Global atmospheric moisture transport associated with precipitation extremes: Mechanisms and climate change impacts. *WIREs Water*, 7(2). <https://doi.org/10.1002/wat2.1412>
- Liu, T., Chen, Y., Chen, S., Li, W., & Zhang, A. (2023). Mechanisms of the transport height of water vapor by tropical cyclones on heavy rainfall. *Weather and Climate Extremes*, 41, 100587. <https://doi.org/10.1016/j.wace.2023.100587>
- Lu, M., & Hao, X. (2017). Diagnosis of the tropical moisture exports to the mid-latitudes and the role of atmospheric steering in the extreme precipitation. *Atmosphere*, 8(12), 256. <https://doi.org/10.3390/atmos8120256>
- Lu, M., & Lall, U. (2017). Tropical moisture exports, extreme precipitation and floods in northeastern US. *Earth Science Research*, 6(2), 91. <https://doi.org/10.5539/esr.v6n2p91>
- Lu, X., Yu, H., Ying, M., Zhao, B., Zhang, S., Lin, L., et al. (2021). Western North Pacific tropical cyclone database created by the China Meteorological Administration. *Advances in Atmospheric Sciences*, 38(4), 690–699. <https://doi.org/10.1007/s00376-020-0211-7>
- Massicotte, P., & Markager, S. (2016). Using a Gaussian decomposition approach to model absorption spectra of chromophoric dissolved organic matter. *Marine Chemistry*, 180, 24–32. <https://doi.org/10.1016/j.marchem.2016.01.008>
- Moore, B. J., Bosart, L. F., Keyser, D., & Jurewicz, M. L. (2013). Synoptic-scale environments of predecessor rain events occurring east of the rocky mountains in association with Atlantic basin tropical cyclones. *Monthly Weather Review*, 141(3), 1022–1047. <https://doi.org/10.1175/mwr-d-12-00178.1>
- Musgrave, K. D., Taft, R. K., Vigh, J. L., McNoldy, B. D., & Schubert, W. H. (2012). Time evolution of the intensity and size of tropical cyclones. *Journal of Advances in Modeling Earth Systems*, 4(3). <https://doi.org/10.1029/2011ms000104>
- Nayak, M. A., & Villarini, G. (2017). A long-term perspective of the hydroclimatological impacts of atmospheric rivers over the central United States. *Water Resources Research*, 53(2), 1144–1166. <https://doi.org/10.1002/2016wr019033>
- Pan, M., & Lu, M. (2019). A novel atmospheric river identification algorithm. *Water Resources Research*, 55(7), 6069–6087. <https://doi.org/10.1029/2018wr024407>
- Park, C., Son, S. W., & Kim, H. (2021). Distinct features of atmospheric rivers in the early versus late East Asian summer monsoon and their impacts on monsoon rainfall. *Journal of Geophysical Research: Atmospheres*, 126(7), e2020JD033537. <https://doi.org/10.1029/2020jd033537>
- Pickl, M., Quinting, J. F., & Grams, C. M. (2023). Warm conveyor belts as amplifiers of forecast uncertainty. *Quarterly Journal of the Royal Meteorological Society*, 149(756), 3064–3085. <https://doi.org/10.1002/qj.4546>
- Pradhan, R. K., Markonis, Y., Vargas Godoy, M. R., Villalba-Pradas, A., Andreadis, K. M., Nikolopoulos, E. I., et al. (2022). Review of GPM IMERG performance: A global perspective. *Remote Sensing of Environment*, 268, 112754. <https://doi.org/10.1016/j.rse.2021.112754>

- Rutz, J. J., Shields, C. A., Lora, J. M., Payne, A. E., Guan, B., Ullrich, P., et al. (2019). The atmospheric river tracking method intercomparison project (ARTMIP): Quantifying uncertainties in atmospheric river climatology. *Journal of Geophysical Research: Atmospheres*, *124*(24), 13777–13802. <https://doi.org/10.1029/2019jd030936>
- Saito, K. (2019). On the northward ageostrophic winds associated with a tropical cyclone. *Sola*, *15*(0), 222–227. <https://doi.org/10.2151/sola.2019-040>
- Saito, K., & Matsunobu, T. (2020). Northward ageostrophic winds associated with a tropical cyclone. Part 2: Moisture transport and its impact on PRE. *Sola*, *16*(0), 198–205. <https://doi.org/10.2151/sola.2020-034>
- Saito, K., Matsunobu, T., & Oizumi, T. (2022). Effect of upper-air moistening by northward ageostrophic winds associated with a tropical cyclone on the PRE enhancement. *Sola*, *18*(0), 81–87. <https://doi.org/10.2151/sola.2022-014>
- Schumacher, R. S., Galarneau, T. J., & Bosart, L. F. (2011). Distant effects of a recurring tropical cyclone on rainfall in a midlatitude convective system: A high-impact predecessor rain event. *Monthly Weather Review*, *139*(2), 650–667. <https://doi.org/10.1175/2010mwr3453.1>
- Sun, Y., Zhong, Z., Li, T., Yi, L., Hu, Y., Wan, H., et al. (2017). Impact of ocean warming on tropical cyclone size and its destructiveness. *Scientific Reports*, *7*(1), 8154. <https://doi.org/10.1038/s41598-017-08533-6>
- Tang, C. K., & Chan, J. C. L. (2013). Idealized simulations of the effect of Taiwan and Philippines topographies on tropical cyclone tracks. *Quarterly Journal of the Royal Meteorological Society*, *140*(682), 1578–1589. <https://doi.org/10.1002/qj.2240>
- Wang, S., Ma, X., Zhou, S., Wu, L., Wang, H., Tang, Z., et al. (2023). Extreme atmospheric rivers in a warming climate. *Nature Communications*, *14*(1), 3219. <https://doi.org/10.1038/s41467-023-38980-x>
- Wen, Y., Xue, L., Li, Y., Wei, N., & Lü, A. (2015). Interaction between Typhoon Vicente (1208) and the western Pacific subtropical high during the Beijing extreme rainfall of 21 July 2012. *Journal of Meteorological Research*, *29*(2), 293–304. <https://doi.org/10.1007/s13351-015-4097-8>
- Xiao, S., Zhang, A., Chen, Y., & Li, W. (2024). Objective identification of tropical cyclone-induced remote moisture transport using digraphs. *Quarterly Journal of the Royal Meteorological Society*, *150*(758), 559–575. <https://doi.org/10.1002/qj.4612>
- Xie, S.-P., Mei, W., Zhao, M., & Wang, Y. (2015). Forced and internal variability of tropical cyclone track density in the western North Pacific. *Journal of Climate*, *28*(1), 143–167. <https://doi.org/10.1175/jcli-d-14-00164.1>
- Xu, H., Duan, Y., & Xu, X. (2022). Indirect effects of binary typhoons on an extreme rainfall event in Henan Province, China from 19 to 21 July 2021: I. Ensemble-Based analysis. *Journal of Geophysical Research: Atmospheres*, *127*(10), e2021JD036265. <https://doi.org/10.1029/2021jd036265>
- Xu, H., Li, X., Yin, J., & Zhang, D. (2023). Predecessor rain events in the Yangtze River Delta region associated with South China Sea and northwest Pacific Ocean (SCS-WNPO) tropical cyclones. *Advances in Atmospheric Sciences*, *40*(6), 1021–1042. <https://doi.org/10.1007/s00376-022-2069-3>
- Yin, J., Gu, H., Liang, X., Yu, M., Sun, J., Xie, Y., et al. (2022). A possible dynamic mechanism for rapid production of the extreme hourly rainfall in Zhengzhou City on 20 July 2021. *Journal of Meteorological Research*, *36*(1), 6–25. <https://doi.org/10.1007/s13351-022-1166-7>
- Yin, L., Ping, F., Mao, J., & Jin, S. (2022). Analysis on precipitation efficiency of the “21.7” Henan extremely heavy rainfall event. *Advances in Atmospheric Sciences*, *40*(3), 374–392. <https://doi.org/10.1007/s00376-022-2054-x>
- Yin, Y., Yong, Y., Qi, S., Yang, K., & Lan, Y. (2023). Cluster analyses of tropical cyclones with genesis in the South China Sea based on K-means method. *Asia-Pacific Journal of Atmospheric Sciences*, *59*(4), 433–446. <https://doi.org/10.1007/s13143-023-00322-8>
- Yu, J., Gao, S., Zhang, L., Shen, X., & Guo, L. (2020). Analysis of a remote rainstorm in the Yangtze River Delta region caused by Typhoon Mangkhut (2018). *Journal of Marine Science and Engineering*, *8*(5), 345. <https://doi.org/10.3390/jmse8050345>
- Zuo, H., Chen, Y., Chen, S., Li, W., & Zhang, A. (2022). The effect of the water tower of Typhoon Mangkhut (2018). *Atmosphere*, *13*(4), 636. <https://doi.org/10.3390/atmos13040636>